electronics

Article

Rational Distributed Bragg Reflector Design for Improving Performance of Flip-Chip Micro-LEDs

Yuechang Sun, Lang Shi, Peng Du, Xiaoyu Zhao and Shengjun Zhou *

Center for Photonics and Semiconductors, School of Power and Mechanical Engineering, Wuhan University, Wuhan 430072, China

* Correspondence: zhousj@whu.edu.cn; Tel.: +86-027-5085-3293

Abstract: The distributed Bragg reflector (DBR) has been widely used in flip-chip micro light-emitting diodes (micro-LEDs) because of its high reflectivity. However, the conventional double-stack DBR has a strong angular dependence and a narrow reflective bandwidth. Here, we propose a wide reflected angle Ti_3O_5/SiO_2 DBR (WRA-DBR) for AlGaInP-based red and GaN-based green/blue flip-chip micro-LEDs (RGB flip-chip micro-LEDs) to overcome the drawbacks of the double-stack DBR. The WRA-DBR consisting of six sub-DBRs has high reflectivity within the visible light wavelength region at an incident angle of light ranging from 0° to 60°. Furthermore, the influence of the WRA-DBR and double-stack DBR on performances of RGB flip-chip micro-LEDs is numerically investigated based on the finite-difference time-domain method. Owing to higher reflectivity and less angular dependence of the WRA-DBR, the RGB flip-chip micro-LEDs with the WRA-DBR have a stronger electric field intensity in the top side in comparison with RGB flip-chip micro-LEDs with the double-stack DBR, which indicates that more photons can be extracted from micro-LEDs with the WRA-DBR.

Keywords: distributed Bragg reflector; flip-chip; micro-LED; FDTD

check for updates

Citation: Sun, Y.; Shi, L.; Du, P.; Zhao, X.; Zhou, S. Rational Distributed Bragg Reflector Design for Improving Performance of Flip-Chip Micro-LEDs. *Electronics* **2022**, *11*, 3030. https://doi.org/10.3390/electronics11193030

Academic Editor: Lucas Lamata

Received: 3 September 2022
Accepted: 20 September 2022
Published: 23 September 2022

1. Introduction

Micro light-emitting diodes (micro-LEDs) have been highlighted as a promising candidate for the realization of next-generation display panels with high dynamic range (HDR) and high resolution because of their numerous advantages such as high luminance, outstanding power efficiency, fast response time, stability, long lifetime, and wide color gamut [1–9]. The full-color micro-LED display panels can be realized by a combination of efficient red, green, and blue micro-LEDs (RGB micro-LEDs) [10–13]. However, to realize the above applications, the external quantum efficiency (EQE) of RGB micro-LEDs should be further improved. A number of methods applied to broad-area LEDs for improving the efficiency could also be applied to micro-LEDs, such as flip-chip technology [6,14–20], surface roughening [21,22], chip shaping [23–25], and patterned sapphire substrate (PSS) [26–29]. Among these methods, flip-chip technology is widely used in micro-LEDs due to its advantage in light extraction efficiency (LEE), heat dissipation, and current spreading.

It is well known that the light generated in the multiple quantum wells (MQWs) active region emits in all directions. In flip-chip micro-LEDs, we expect that light emits to air mainly from the top substrates. However, a myriad of light generated in MQWs travels downward, which does not make any contributions to the LEE. A bottom reflector plays an essential role in improving the LEE by reflecting the light back into the top substrates. The distributed Bragg reflector (DBR) has been extensively used as the bottom reflector owing to its high reflectivity in a specific wavelength region [30–32]. A typical DBR is made by stacking low refractive index dielectric layers (e.g., SiO_2) and high refractive index dielectric layers (e.g., TiO_2 and Ti_3O_5), exhibiting a low absorption in the visible light region. Five pairs of TiO_2/SiO_2 single-stack DBR designed for GaN-based green LEDs exhibited that the reflective bandwidth with a high reflectivity (>80%) was larger than

100 nm [31]. A double-stack DBR optimized for two different central wavelengths was designed to provide a higher reflectivity and a larger reflective bandwidth in comparison with a single-stack DBR [33]. Nevertheless, the double-stack DBR still shows severe angular dependence, which hinders further improvement of LEE in flip-chip micro-LEDs. A full-angle DBR composed of 14 sub-DBRs optimized for central wavelength in blue, green, and red wavelength regions exhibited a wide reflective bandwidth and alleviated the angular dependence [34]. However, the reflective bandwidth of the full-angle DBR is limited in the blue and green light wavelength region, which is not suitable for red micro-LEDs. Therefore, to improve the performance of the RGB flip-chip micro-LEDs, a DBR with wider reflective bandwidth covering the whole visible light wavelength region and less angular dependence is required.

To overcome the above-mentioned drawbacks of the DBRs, we propose a wide reflected angle Ti_3O_5/SiO_2 DBR (WRA-DBR). The WRA-DBR is composed of six sub-DBRs optimized for different central wavelengths ranging from the blue light wavelength region to the red light wavelength region. The WRA-DBR has a superior reflectivity within the whole visible light region and exhibits less angular dependence. The average reflectivity of the WRA-DBR at a normal incident angle of light within the wavelength region from 400 nm to 700 nm can reach up to 99.73%. Furthermore, the average reflectivity of the WRA-DBR is up to 97.93% when the incident angle of light is 60°. Compared to conventional double-stack DBR, the WRA-DBR exhibits a wider reflective bandwidth and alleviates the angular dependence. To further evaluate the effect of the WRA-DBR on the optical performance of RGB micro-LEDs, a simulation was carried out by using finite difference time domain (FDTD) method. The result demonstrates that the WRA-DBR can act as a potential candidate for realizing high-efficiency RGB flip-chip micro-LEDs.

2. Model and Methods

The DBR, based on the thin-film interference effect, is an array of multilayer stacks composed of two kinds of dielectric layers with high and low refractive indices. The dielectric layer thickness can be calculated by the following formula [35]:

$$n_1 t_1 = n_2 t_2 = \lambda/4, \tag{1}$$

where the n_1 and n_2 are refractive indices of the high refractive layer and the low refractive layer, respectively, the t_1 and t_2 are thicknesses of the high refractive layer and the low refractive layer, respectively, and λ is the central wavelength.

Figure 1a shows the schematic illustration of the single-stack DBR. The single-stack DBR consists of N periods of layer 1 and layer 2. The refractive indices of layer 1 and layer 2 are n_1 and n_2, respectively. The thicknesses of layer 1 and layer 2 are t_1 and t_2, respectively. We consider the refractive indices of the incident medium and the substrate are n_0 and n_3, respectively. The reflection coefficient and reflectivity of the single-stack DBR can be calculated based on the transfer matrix method (TMM). From the TMM, the total transfer matrix M can be calculated according to the following equation [36,37]:

$$\boldsymbol{M} = \begin{pmatrix} M_{11} & M_{12} \\ M_{21} & M_{22} \end{pmatrix} = \boldsymbol{D}_0^{-1}\left[\boldsymbol{D}_1\boldsymbol{P}_1\boldsymbol{D}_1^{-1}\boldsymbol{D}_2\boldsymbol{P}_2\boldsymbol{D}_2^{-1}\right]^N\boldsymbol{D}_3 \tag{2}$$

the reflection coefficient can be expressed as

$$r = \frac{M_{21}}{M_{11}}, \tag{3}$$

the dynamical matrix for the medium α can be expressed as [36,37]

$$D_\alpha = \begin{cases} \begin{pmatrix} 1 & 1 \\ n_\alpha \cos\theta_\alpha & -n_\alpha \cos\theta_\alpha \end{pmatrix} \text{for TE wave} \\ \begin{pmatrix} \cos\theta_\alpha & \cos\theta_\alpha \\ n_\alpha & -n_\alpha \end{pmatrix} \text{for TM wave} \end{cases}, \ \alpha = 0,\ 1,\ 2 \text{ and } 3 \tag{4}$$

the propagation matrix is given by

$$P_\alpha = \begin{pmatrix} \exp(i\phi_\alpha) & 0 \\ 0 & \exp(-i\phi_\alpha) \end{pmatrix},\ \alpha = 1,\ 2 \tag{5}$$

and

$$\phi_\alpha = \frac{2\pi}{\lambda} n_\alpha t_\alpha \cos\theta_\alpha,\ \alpha = 1,\ 2 \tag{6}$$

where λ is the wavelength of incident light, and θ_α is the incident angle of light in the dielectric layer calculated by Snell's law of refraction:

$$n_0 \sin\theta_0 = n_1 \sin\theta_1 = n_2 \sin\theta_2 = n_3 \sin\theta_3 \tag{7}$$

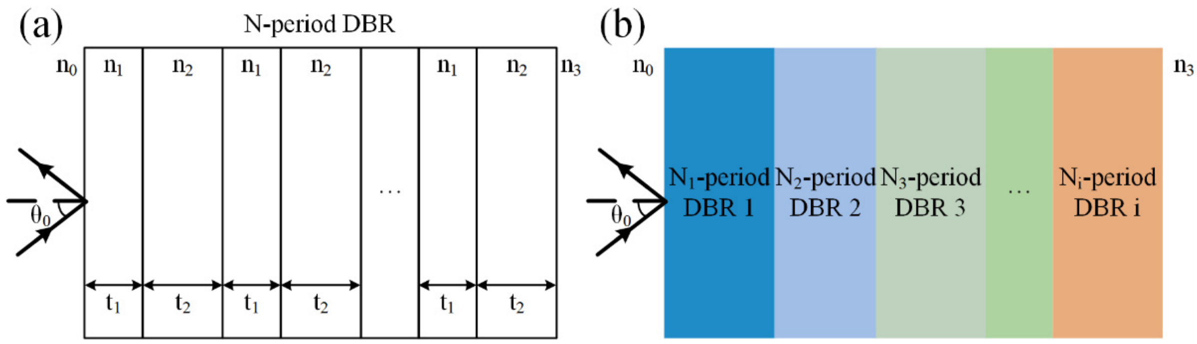

Figure 1. (**a**) Schematic illustration of a single-stack DBR consisting of N periods of layer 1 and layer 2. (**b**) Schematic illustration of DBR consisting of several sub-DBRs. Ni (i = 1, 2, 3 . . .) is the periods of the sub-DBRs.

Then, the reflectivity of the single-stack DBR can be calculated by the following equation:

$$R = r^2 \tag{8}$$

Figure 1b shows the schematic illustration of the DBR consisting of several single-stack DBRs (sub-DBRs). N_i (i = 1, 2, 3 . . .) is the periods of the sub-DBRs. The total transfer matrix of the DBR is

$$M = \begin{pmatrix} M_{11} & M_{12} \\ M_{21} & M_{22} \end{pmatrix} = D_0^{-1}\left[D_1 P_1 D_1^{-1} D_2 P_2 D_2^{-1}\right]^{N1} \cdots \left[D_1 P_1 D_1^{-1} D_2 P_2 D_2^{-1}\right]^{Ni} D_3 \tag{9}$$

Then, the reflectivity of the DBR can be calculated from the above-mentioned equations.

3. Results and Discussion

Based on TMM, we investigate the angular dependence and reflective bandwidth of the double-stack Ti_3O_5/SiO_2 DBR. The double-stack Ti_3O_5/SiO_2 DBR is designed and modeled by TFCalc software. The double-stack DBR consists of two sub-DBRs, which are composed of 12 periods of Ti_3O_5/SiO_2. The refractive indices of Ti_3O_5 and SiO_2 in the simulation are fixed at 2.37 and 1.46, respectively. The central wavelengths of the two sub-DBRs are optimized for 465 nm and 630 nm, respectively. Therefore, the thicknesses of Ti_3O_5/SiO_2 dielectric layers are 48.97 nm/79.68 nm and 66.34 nm/108.00 nm, respectively.

Figure 2a shows the schematic illustration of the double-stack DBR structure. Figure 2b shows the reflectance spectra of the double-stack DBR. The electroluminescent (EL) spectra of red, green, and blue micro-LEDs are also shown in Figure 2b. The peak wavelengths of red, green, and blue micro-LEDs are 630 nm, 520 nm, and 465 nm, respectively. It is clearly seen in Figure 2b that the reflectivity of the double-stack DBR is high within the whole visible light region when the incident angle of light is 0°. However, as the incident angle increases, the reflective bands exhibit a blueshift and the reflectivity decreases sharply in blue and green light wavelength regions. This result indicates that the double-stack DBR has a strong angular dependence.

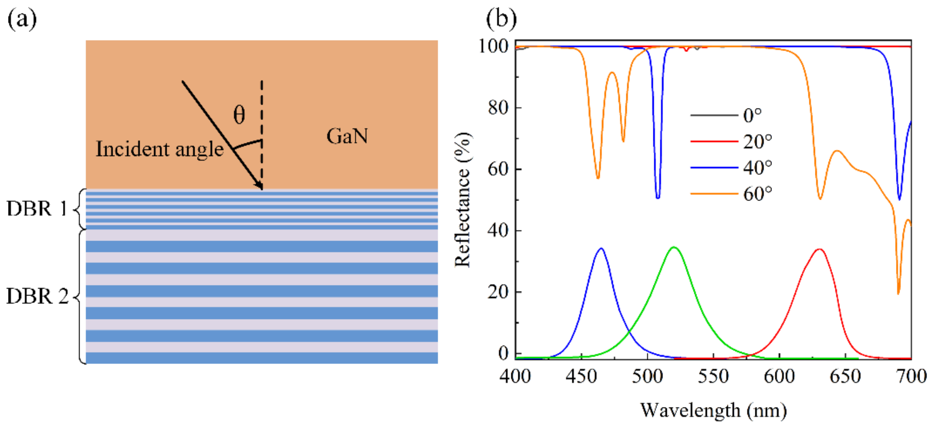

Figure 2. (**a**) Schematic illustration of double-stack DBR structure. (**b**) Reflectance spectra of the double-stack DBR as a function of incident angle.

To suppress the sharp decrease in the reflectivity in blue and green light wavelength regions, DBR III is designed by inserting a sub-DBR stack into the double-stack DBR. The inserted sub-DBR is optimized for a central wavelength at 520 nm, and the thickness of Ti_3O_5/SiO_2 of the inserted sub-DBR is 55.81 nm/90.82 nm. The total periods of DBR III are the same as that of double-stack DBR, which means that DBR III is composed of 24 periods of Ti_3O_5/SiO_2. Therefore, each sub-DBR of DBR III is made of eight periods of Ti_3O_5/SiO_2. Figure 3b shows the reflectance spectra of DBR III as a function of incident angle of light. After adding a sub-DBR, the sharp decrease of reflectivity of the double-stack DBR in the blue and green light wavelength region is alleviated, revealing that the added sub-DBR can broaden the reflective bandwidth. However, the reflectivity of DBR III in the red light wavelength region at a large incident angle of light remains relatively low.

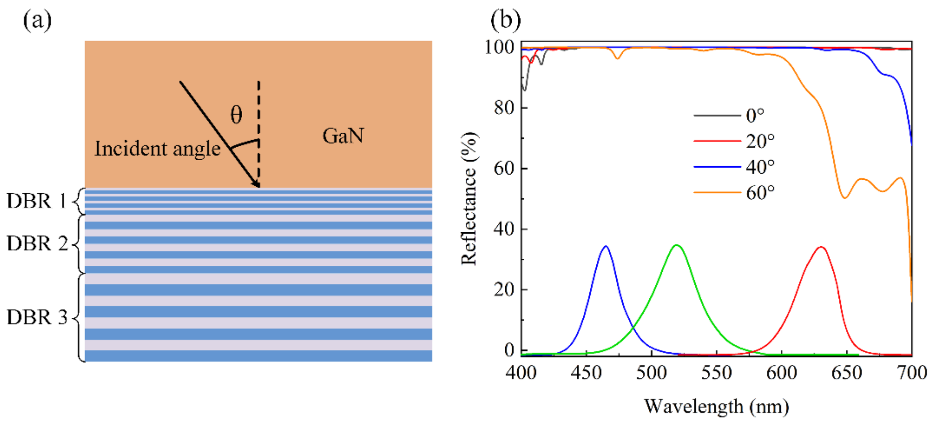

Figure 3. (**a**) Schematic illustration of DBR III structure. (**b**) Reflectance spectra of the DBR III as a function of incident angle.

To further improve the reflectivity of the DBR in the red light wavelength region, DBR IV with a combination of DBR III and another sub-DBR optimized for the central wavelength at 650 nm is designed, and the thickness of Ti_3O_5/SiO_2 of the inserted sub-DBR is 68.45 nm/111.38 nm. Each sub-DBR of DBR IV is composed of six periods of Ti_3O_5/SiO_2. Figure 4a shows the schematic illustration of the DBR IV structure. Figure 4b shows the reflectance of DBR IV. As shown in Figure 4b, the reflectivity is high when the incident angle of light is below 40°. However, the reflectivity of DBR IV at a large incident angle of light is not greatly improved in comparison with DBR III. To further enhance the performance of DBR IV, we investigate the influence of the sub-DBR optimized for different central wavelengths on the reflectivity. Figure 4c shows the reflectance spectra of DBR IV with the added sub-DBR optimized for different central wavelengths when the incident angle of light is 60°. The average reflectivity increases as the central wavelength of the sub-DBR increases from 650 nm to 730 nm. When the central wavelength of the inserted sub-DBR is 730 nm, the average reflectivity of DBR IV is larger than 90%. Therefore, we adopted the inserted sub-DBR optimized for the central wavelength at 730 nm.

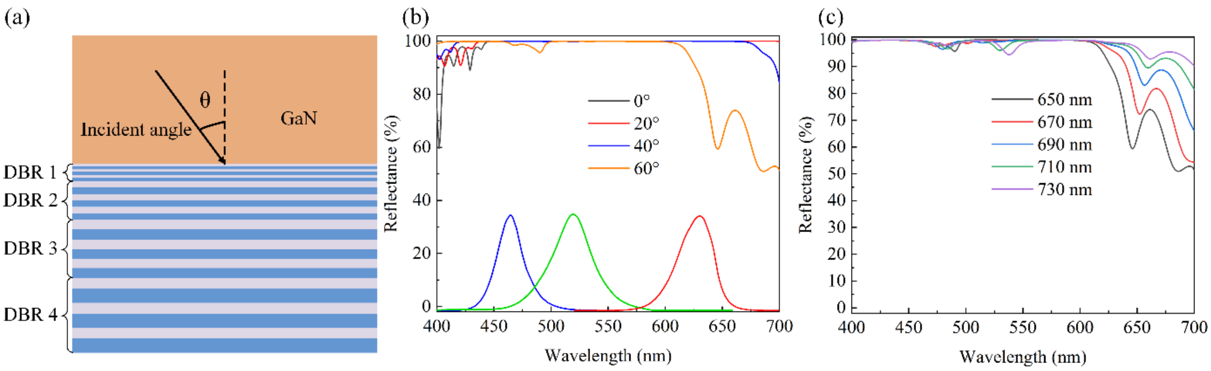

Figure 4. (**a**) Schematic illustration of DBR IV structure; (**b**) reflectance spectra of the DBR IV as a function of incident angle; (**c**) reflectance spectra of DBR IV with an added sub-DBR optimized for different central wavelengths at an incident angle of 60°.

To overcome the drawbacks outlined above, the WRA-DBR structure with a combination of DBR IV and another two sub-DBRs is designed. The thicknesses of Ti_3O_5/SiO_2 of the two sub-DBRs are 46.34 nm/75.39 nm and 78.98 nm/128.51 nm, respectively. Meanwhile, the central wavelengths of sub-DBRs and number of periods of Ti_3O_5/SiO_2 in the WRA-DBR are 440 nm/4 periods, 465 nm/4 periods, 520 nm/4 periods, 630 nm/5 periods, 730 nm/3 periods, and 750 nm/4 periods, respectively. Figure 5a shows the schematic of the WRA-DBR structure. Figure 5b shows the reflectance spectra of the WRA-DBR at different incident angles of light. Among all the mentioned DBRs, the WRA-DBR possesses the widest reflective bandwidth. It should be mentioned that the average reflectivity of the WRA-DBR at a normal incident angle of light is 99.73% within the wavelength region from 400 nm to 700 nm. The reflectivity of the WRA-DBR can reach up to 97.93% within the wavelength region from 400 nm to 700 nm when the incident angle of light is 60°, indicating that the WRA-DBR has alleviated the angular dependence.

We investigate the influence of the double-stack DBR and the WRA-DBR on the performance of RGB flip-chip micro-LEDs using the finite-difference time-domain (FDTD) method. Figure 6 shows the simulation models of the RGB flip-chip micro-LEDs with the double-stack DBR and the WRA-DBR. The optical parameters and the thicknesses of each layer of the RGB flip-chip micro-LEDs are shown in Table 1. The AlGaInP-based red micro-LED consists of ITO, p-GaP, p-AlInP, MQWs, n-AlGaInP, and n-GaAs. The GaN-based green and blue micro-LEDs are composed of ITO, p-GaN, MQWs, and n-GaN. The sidewalls of the RGB micro-LEDs are inclined and the inclination angle is 70° [38]. For simplicity, the metal electrode layer of the micro-LEDs is neglected. Considering the memory of the computer and computing time, the size of micro-LEDs is set to be 8 μm × 8 μm. The perfect matched layer (PML) is used to avoid the reflected electromagnetic wave at the boundary of the micro-LEDs. A 9 × 9 dipole source array is placed in the MQWs as a light source, and the space between dipoles is set to 0.8 μm. The emission wavelengths of the dipole sources in the RGB micro-LEDs are 630 nm, 520 nm, and 465 nm, respectively. A cross-sectional discrete Fourier transform (DFT) monitor is used to obtain the electric field distribution and a transmission box monitor is used to calculate the LEEs. Figure 7a–f show the electric field distributions of RGB flip-chip micro-LEDs with the double-stack DBR and WRA-DBR. In Figure 7a–f, region I is the bottom external space of micro-LEDs and region II is the top external space of the micro-LEDs. According to the electric field distributions shown in Figure 7a–f, it can be observed that there exists a weaker electric field intensity in the WRA-DBR in comparison with the electric field intensity in the double-stack DBR, indicating that the WRA-DBR has a higher reflectivity than the double-stack DBR. Therefore, more photons will be reflected upward to region II. Furthermore, compared to RGB flip-chip micro-LEDs with a double-stack DBR, stronger electric field intensity exists in the air of region II outside the RGB flip-chip micro-LEDs with the WRA-DBR, implying that the photons are more likely to be extracted from RGB flip-chip micro-LEDs with the WRA-DBR. Moreover, the LEEs of each face of the RGB micro-LEDs with the double-stack DBR and WRA-DBR are shown in Figure 7g–i. In Figure 7g, the LEEs of blue micro-LEDs with the double-stack DBR and blue micro-LEDs with the WRA-DBR are almost same. The reason for the similar LEEs in the blue micro-LEDs with the double-stack DBR and WRA-DBR is that the double-stack DBR and WRA-DBR both perform well in the blue light region. From the results of Figures 7h and 7i, it can be observed that green and red micro-LEDs with the WRA-DBR exhibit higher LEEs than green and red micro-LEDs with the double-stack DBR.

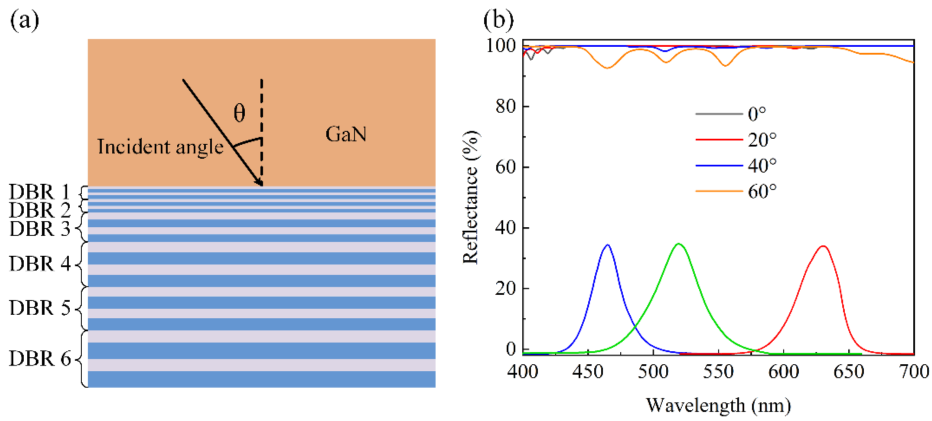

Figure 5. (**a**) Schematic illustration of the WRA-DBR structure. (**b**) Reflectance spectra of the WRA-DBR as a function of incident angle.

Table 1. Optical parameters for each layer of AlGaInP-based red micro-LED and GaN-based blue and green micro-LEDs used in the FDTD simulations.

Red Micro-LED	Thickness (μm)	n	k	Green/Blue Micro-LED	Thickness (μm)	n Green (Blue)	k Green (Blue)
p-GaP	2	3.322	0	p-GaN	0.5	2.38 (2.43)	5×10^{-3} (6×10^{-3})
p-AlInP	0.42	3.014	4×10^{-3}	n-GaN	2.5	2.38 (2.43)	5×10^{-3} (6×10^{-3})
n-AlGaInP	1.3	3.223	9×10^{-3}	ITO	0.28	1.89 (1.95)	4×10^{-3} (6×10^{-3})
n-GaAs	0.08	3.856	0.196	-	-	-	-
ITO	0.28	1.79	0	-	-	-	-

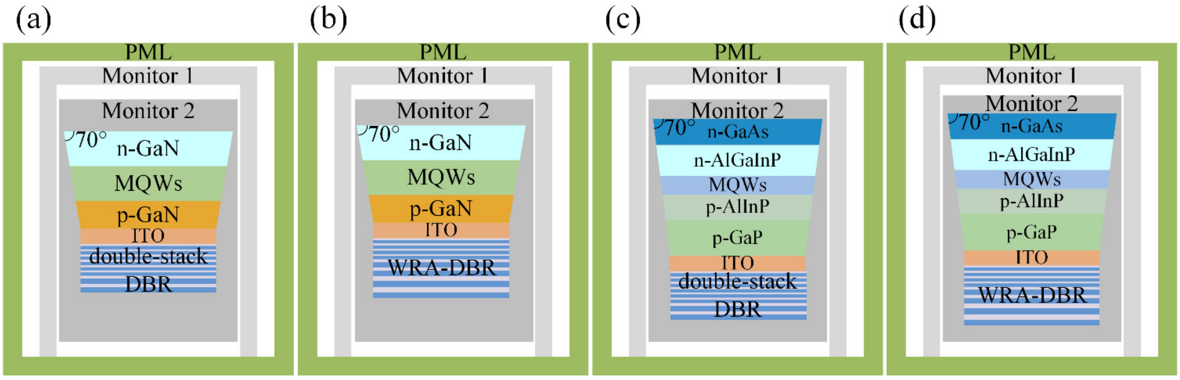

Figure 6. Simulation model of (**a**) blue/green micro-LED with double-stack DBR, (**b**) blue/green micro-LED with WRA-DBR, (**c**) red micro-LED with double-stack DBR, (**d**) red micro-LED with WRA-DBR.

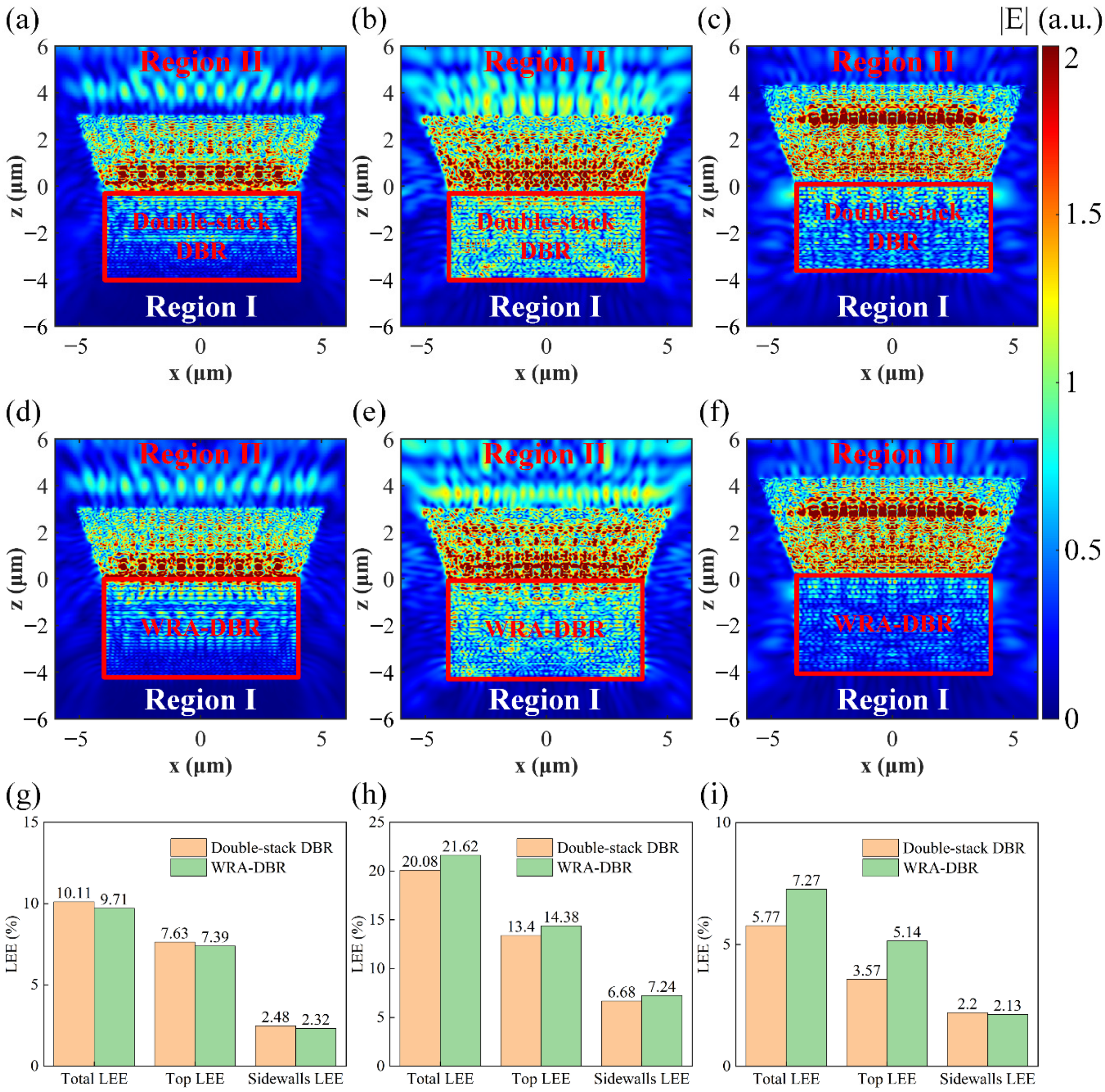

Figure 7. Simulated electric field distributions for a cross section of micro-LEDs: (**a**) blue, (**b**) green, (**c**) red micro-LEDs with double-stack DBR; (**d**) blue, (**e**) green, (**f**) red micro-LEDs with WRA-DBR. LEEs of each face (top and sidewalls) of (**g**) blue, (**h**) green, (**i**) red micro-LEDs with double-stack DBR and WRA-DBR.

4. Conclusions

In summary, we have designed a WRA-DBR consisting of six sub-DBRs with high reflectivity and less angular dependence within the visible light wavelength region. The average reflectivity of the WRA-DBR at a normal incident angle of light can reach up to 99.73% in the wavelength range of 400 nm to 700 nm. Moreover, the average reflectivity of the WRA-DBR is up to 97.93% when the incident angle of light is 60°, revealing that the WRA-DBR has less angular dependence. Furthermore, we investigate the influence of the double-stack DBR and WRA-DBR on the performance of RGB flip-chip micro-LEDs using the FDTD method. Compared to RGB flip-chip micro-LEDs with the double-stack DBR, stronger electric field intensity is found in the air outside the substrates of RGB flip-chip micro-LEDs with the WRA-DBR, indicating that the WRA-DBR can significantly improve the performance of RGB flip-chip micro-LEDs. Our work demonstrates the promising potential of the WRA-DBR for realization of high-efficiency RGB flip-chip micro-LEDs.

Author Contributions: Conceptualization, S.Z.; methodology, Y.S., X.Z. and S.Z.; validation, Y.S. and L.S.; formal analysis, Y.S., L.S. and P.D.; investigation, Y.S., L.S. and S.Z.; data curation, Y.S. and L.S.; writing—original draft preparation, Y.S.; writing—review and editing, S.Z.; visualization, Y.S.; supervision, S.Z.; project administration, S.Z.; funding acquisition, S.Z. All authors have read and agreed to the published version of the manuscript.

Funding: This research was funded by the National Natural Science Foundation of China (52075394) and the National Key R & D Program of China (2021YFB3600200). The authors also acknowledge valuable support from the National Youth Talent Support Program.

Data Availability Statement: The data that support the findings of this study are available from the corresponding author upon reasonable request.

Acknowledgments: The authors also acknowledge valuable support from the National Youth Talent Support Program.

Conflicts of Interest: The authors declare no conflict of interest.

References

1. Huang, Y.M.; Chen, J.H.; Liou, Y.H.; Singh, K.J.; Tsai, W.C.; Han, J.; Lin, C.J.; Kao, T.S.; Lin, C.C.; Chen, S.C.; et al. High-Uniform and High-Efficient Color Conversion Nanoporous GaN-Based Micro-LED Display with Embedded Quantum Dots. *Nanomaterials* **2021**, *11*, 2696. [CrossRef] [PubMed]
2. Hsiang, E.L.; He, Z.; Huang, Y.; Gou, F.; Lan, Y.F.; Wu, S.T. Improving the Power Efficiency of Micro-LED Displays with Optimized LED Chip Sizes. *Crystals* **2020**, *10*, 494. [CrossRef]
3. Kishino, K.; Sakakibara, N.; Narita, K.; Oto, T. Two-dimensional multicolor (RGBY) integrated nanocolumn micro-LEDs as a fundamental technology of micro-LED display. *Appl. Phys. Express* **2019**, *13*, 014003. [CrossRef]
4. Gou, F.; Hsiang, E.L.; Tan, G.; Chou, P.T.; Li, Y.L.; Lan, Y.F.; Wu, S.T. Angular color shift of micro-LED displays. *Opt. Express* **2019**, *27*, A746–A757. [CrossRef]
5. Horng, R.H.; Chien, H.Y.; Tarntair, F.G.; Wuu, D.S. Fabrication and Study on Red Light Micro-LED Displays. *IEEE J. Electron Devices Soc.* **2018**, *6*, 1064–1069. [CrossRef]
6. Chang, K.P.; Tsai, Y.T.; Yen, C.C.; Horng, R.H.; Wuu, D.S. Structural design and performance improvement of flip-chip AlGaInP mini light-emitting diodes. *Semicond. Sci. Technol.* **2021**, *36*, 095008. [CrossRef]
7. Kim, T.K.; Islam, A.; Cha, Y.J.; Kwak, J.S. 32 × 32 Pixelated High-Power Flip-Chip Blue Micro-LED-on-HFET Arrays for Submarine Optical Communication. *Nanomaterials* **2021**, *11*, 3045. [CrossRef]
8. Huang, Y.; Hsiang, E.L.; Deng, M.Y.; Wu, S.T. Mini-LED, Micro-LED and OLED displays: Present status and future perspectives. *Light Sci. Appl.* **2020**, *9*, 105. [CrossRef]
9. Xiong, J.; Hsiang, E.L.; He, Z.; Zhan, T.; Wu, S.T. Augmented reality and virtual reality displays: Emerging technologies and future perspectives. *Light Sci. Appl.* **2021**, *10*, 216. [CrossRef]
10. Wu, Y.; Ma, J.; Su, P.; Zhang, L.; Xia, B. Full-Color Realization of Micro-LED Displays. *Nanomaterials* **2020**, *10*, 2482. [CrossRef]
11. Peng, D.; Zhang, K.; Chao, V.S.D.; Mo, W.; Lau, K.M.; Liu, Z. Full-Color Pixelated-Addressable Light Emitting Diode on Transparent Substrate (LEDoTS) Micro-Displays by CoB. *J. Display Technol.* **2016**, *12*, 742–746. [CrossRef]
12. Zhou, X.; Tian, P.; Sher, C.W.; Wu, J.; Liu, H.; Liu, R.; Kuo, H.C. Growth, transfer printing and colour conversion techniques towards full-colour micro-LED display. *Prog. Quantum Electron.* **2020**, *71*, 100263. [CrossRef]
13. Ding, K.; Avrutin, V.; Izyumskaya, N.; Özgür, Ü.; Morkoç, H. Micro-LEDs, a Manufacturability Perspective. *Appl. Sci.* **2019**, *9*, 1206. [CrossRef]

14. Zhou, S.; Liu, X.; Yan, H.; Chen, Z.; Liu, Y.; Liu, S. Highly efficient GaN-based high-power flip-chip light-emitting diodes. *Opt. Express* **2019**, *27*, A669–A692. [CrossRef] [PubMed]
15. Zhao, P.; Zhao, H. Analysis of light extraction efficiency enhancement for thin-film-flip-chip InGaN quantum wells light-emitting diodes with GaN micro-domes. *Opt. Express* **2012**, *20*, A765–A776. [CrossRef] [PubMed]
16. Jiang, P.; Peng, Y.; Mou, Y.; Cheng, H.; Chen, M.; Liu, S. Thermally stable multi-color phosphor-in-glass bonded on flip-chip UV-LEDs for chromaticity-tunable WLEDs. *Appl. Opt.* **2017**, *56*, 7921–7926. [CrossRef]
17. Konoplev, S.S.; Bulashevich, K.A.; Karpov, S.Y. From Large-Size to Micro-LEDs: Scaling Trends Revealed by Modeling. *Phys. Status Solidi Appl. Mater. Sci.* **2018**, *215*, 1700508. [CrossRef]
18. Liu, X.; Zhou, S.; Gao, Y.; Hu, H.; Liu, Y.; Gui, C.; Liu, S. Numerical simulation and experimental investigation of GaN-based flip-chip LEDs and top-emitting LEDs. *Appl. Opt.* **2017**, *56*, 9502–9509. [CrossRef]
19. Shchekin, O.B.; Epler, J.E.; Trottier, T.A.; Margalith, T.; Steigerwald, D.A.; Holcomb, M.O.; Martin, P.S.; Krames, M.R. High performance thin-film flip-chip InGaN–GaN light-emitting diodes. *Appl. Phys. Lett.* **2006**, *89*, 071109. [CrossRef]
20. Hu, H.; Tang, B.; Wan, H.; Sun, H.; Zhou, S.; Dai, J.; Chen, C.; Liu, S.; Guo, L.J. Boosted ultraviolet electroluminescence of InGaN/AlGaN quantum structures grown on high-index contrast patterned sapphire with silica array. *Nano Energy* **2020**, *69*, 104427. [CrossRef]
21. Tang, B.; Miao, J.; Liu, Y.; Zhou, S.; Xu, H.; Wan, H. Insights into the Influence of Sidewall Morphology on the Light Extraction Efficiency of Mini-LEDs. *IEEE Photon. J.* **2019**, *11*, 8200907. [CrossRef]
22. Guo, Y.; Zhang, Y.; Yan, J.; Xie, H.; Liu, L.; Chen, X.; Hou, M.; Qin, Z.; Wang, J.; Li, J. Light extraction enhancement of AlGaN-based ultraviolet light-emitting diodes by substrate sidewall roughening. *Appl. Phys. Lett.* **2017**, *111*, 011102. [CrossRef]
23. Zhuang, Z.; Iida, D.; Ohkawa, K. Effects of size on the electrical and optical properties of InGaN-based red light-emitting diodes. *Appl. Phys. Lett.* **2020**, *116*, 173501. [CrossRef]
24. Smith, J.M.; Ley, R.; Wong, M.S.; Baek, Y.H.; Kang, J.H.; Kim, C.H.; Gordon, M.J.; Nakamura, S.; Speck, J.S.; DenBaars, S.P. Comparison of size-dependent characteristics of blue and green InGaN microLEDs down to 1 µm in diameter. *Appl. Phys. Lett.* **2020**, *116*, 071102. [CrossRef]
25. Lu, S.; Zhang, Y.; Zhang, Z.H.; Zhu, B.; Zheng, H.; Tan, S.T.; Demir, H.V. High-Performance Triangular Miniaturized-LEDs for High Current and Power Density Applications. *ACS Photon.* **2021**, *8*, 2304–2310. [CrossRef]
26. Chao, S.H.; Yeh, L.H.; Wu, R.T.; Kawagishi, K.; Hsu, S.C. Novel patterned sapphire substrates for enhancing the efficiency of GaN-based light-emitting diodes. *RSC Adv.* **2020**, *10*, 16284–16290. [CrossRef]
27. Manley, P.; Walde, S.; Hagedorn, S.; Hammerschmidt, M.; Burger, S.; Becker, C. Nanopatterned sapphire substrates in deep-UV LEDs: Is there an optical benefit? *Opt. Express* **2020**, *28*, 3619–3635. [CrossRef]
28. Ooi, Y.K.; Zhang, J. Light Extraction Efficiency Analysis of Flip-Chip Ultraviolet Light-Emitting Diodes with Patterned Sapphire Substrate. *IEEE Photon. J.* **2018**, *10*, 8200913. [CrossRef]
29. Zhou, S.; Liu, S. *III-Nitride LEDs: From UV to Green*; Springer Nature: Singapore, 2022; pp. 91–95.
30. Wang, D.X.; Ferguson, I.T.; Buck, J.A. GaN-based distributed Bragg reflector for high-brightness LED and solid-state lighting. *Appl. Opt.* **2007**, *46*, 4763–4767. [CrossRef]
31. Huang, S.Y.; Horng, R.H.; Wang, W.K.; Wuu, D.S. GaN-Based Green Resonant Cavity Light-Emitting Diodes. *Jpn. J. Appl. Phys.* **2006**, *45*, 3433–3435. [CrossRef]
32. Zhi, T.; Tao, T.; Liu, B.; Yan, Y.; Xie, Z.; Zhao, H.; Chen, D. High Performance Wide Angle DBR Design for Optoelectronic Devices. *IEEE Photon. J.* **2021**, *13*, 8200206. [CrossRef]
33. Ding, X.; Gui, C.; Hu, H.; Liu, M.; Liu, X.; Lv, J.; Zhou, S. Reflectance bandwidth and efficiency improvement of light-emitting diodes with double-distributed Bragg reflector. *Appl. Opt.* **2017**, *56*, 4375–4380. [CrossRef] [PubMed]
34. Shi, L.; Zhao, X.; Du, P.; Liu, Y.; Lv, Q.; Zhou, S. Enhanced performance of GaN-based visible flip-chip mini-LEDs with highly reflective full-angle distributed Bragg reflectors. *Opt. Express* **2021**, *29*, 42276–42286. [CrossRef]
35. Kats, M.A.; Blanchard, R.; Genevet, P.; Capasso, F. Nanometre optical coatings based on strong interference effects in highly absorbing media. *Nat. Mater.* **2013**, *12*, 20–24. [CrossRef]
36. Wu, C.J.; Chu, B.H.; Weng, M.T. Analysis of Optical Reflection in a Chirped Distributed Bragg Reflector. *J. Electromagn. Waves Appl.* **2009**, *23*, 129–138. [CrossRef]
37. Pérez, E.X. Design, Fabrication and Characterization of Porous Silicon Multilayer Optical Devices. Ph.D. Thesis, Universitat Rovira i Virgili, Tarragona, Spain, 2008.
38. Hu, X.; Cai, J.; Liu, Y.; Zhao, M.; Chen, E.; Sun, J.; Yan, Q.; Guo, T. Design of inclined omni-directional reflector for sidewall-emission-free micro-scale light-emitting diodes. *Opt. Laser Technol.* **2022**, *154*, 108335. [CrossRef]